Highly transparent superconducting-normal junctions induced by local fields of magnetic domains in a homogeneous superconductor

J. Fritzsche, R. B. G. Kramer, and V. V. Moshchalkov
INPAC-Institute for Nanoscale Physics and Chemistry, Katholieke Universiteit Leuven, Celestijnenlaan 200 D, B-3001 Leuven, Belgium
(Received 5 March 2009; revised manuscript received 24 June 2009; published 18 September 2009)

Using the highly inhomogeneous fields of a magnetic substrate, tunable junctions between superconducting and normal-state regions were created inside a thin-film superconductor. The investigation of these junctions, created *in the same material*, gave evidence for the occurrence of Andreev reflection, indicating the high transparency of interfaces between superconducting and normal-state regions. For the realization of this study, a ferromagnet with magnetic-stripe domains was used as a substrate, on top of which a superconducting transport bridge was prepared perpendicular to the underlying domains. The particular choice of materials allowed to restrict the nucleation of superconductivity to regions above either reverse domains or domain walls. Moreover, due to the specific design of the sample, transport currents in the superconductor passed through a sequence of normal and superconducting regions.

DOI: 10.1103/PhysRevB.80.094514 PACS number(s): 74.45.+c, 74.78.Db, 75.60.Ch

I. INTRODUCTION

There is a wealth of physical phenomena inherent to junctions between superconducting (S) and normal (N) matter, such as the Josephson effect,[1] quasiparticle tunneling,[2] and Andreev reflection (AR).[3,4] Traditionally, SN junctions are either based on composites of superconducting and normal-conducting materials, or on constrictions/thickness modulations of superconducting films. A common feature of these junctions is their fixed character since they are static constructions that cannot be modified any more once they are fabricated. However, recent works have shown that the highly inhomogeneous fields of ferromagnetic domains can be used to locally suppress superconductivity in thin S films, resulting in the states of domain-wall superconductivity (DWS) (Ref. 5) or reverse-domain superconductivity (RDS).[6] In these two states, the superconductor can be seen as a network of SN junctions, which can exhibit the same flexibility as the underlying magnetic domains. In this paper, we demonstrate that tunable SN junctions can be created in a controlled way by using the highly inhomogeneous fields of ferromagnetic domains. In particular, we show that in such junctions, the interfaces between the superconducting and the normal parts are highly transparent for incident electrons, which is a consequence of creating superconducting and normal-state regions inside the *same material*.

In order to experimentally investigate SN interfaces that are induced by stray magnetic fields, a specially designed superconductor/ferromagnet (S/F) hybrid[7–9] system was needed, exhibiting the following two qualities: (i) the opportunity to specifically realize superconductivity either above the magnetic domain walls (DWS) or above the reverse domains (RDS) of the substrate. (ii) Transport currents had to cross effectively the interfaces between the induced superconducting and normal-state regions. The preparation of such system is challenging as several strict requirements need to be fulfilled. First of all, formation of magnetic-stripe domains in the template is desirable.[10] Alignment of a transport bridge perpendicular to such domains guarantees a bias current to cross them successively. Second, the magnetic domain pattern of the template must not change significantly when subjected to external fields, required for setting up the different states (e.g., RDS) in the S layer. Finally, the out-of plane component of the stray field above magnetic domains has to reach the upper critical field of the superconductor.[11] Thereby, realization of DWS is possible down to temperatures well below T_c.

II. EXPERIMENTAL

Accounting for the above requirements, S/F hybrid systems were prepared by slicing a single crystal of barium hexaferrite ($BaFe_{12}O_{19}$) under a small tilt to its *c* axis [Fig. 1(b)] and then processing superconducting aluminum bridges of 50 nm thickness on the cut surfaces perpendicular to the *c* axis [Fig. 1(d)]. The superconducting and ferromagnetic components were electrically isolated by 5 nm SiO_2 in order

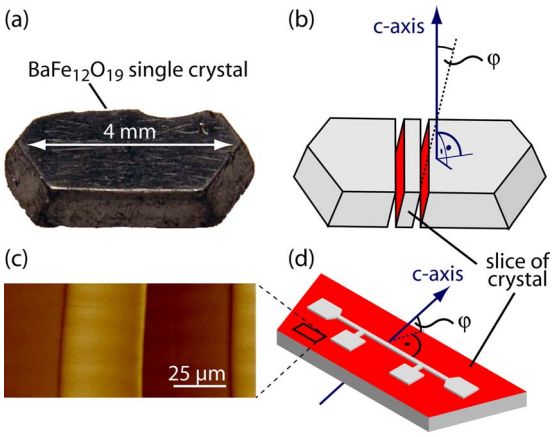

FIG. 1. (Color online) (a) Photograph of the as-grown barium hexaferrite single crystal. (b) Sketch of the crystal after slicing under a cut angle φ with respect to its *c* axis. (c) Magnetic-force microscopical image of the magnetic domains at the cut surface of a slice of the $BaFe_{12}O_{19}$ single crystal. (d) Sketch of a transport bridge processed perpendicular to the *c* axis on the cut surface of a slice of the crystal.

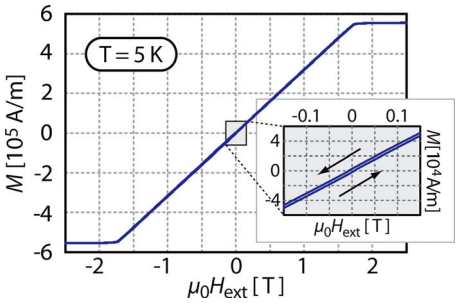

FIG. 2. (Color online) The magnetization M of a slice of the $BaFe_{12}O_{19}$ single crystal at 5 K as a function of the external magnetic field $\vec{H}_{ext}$ normal to the cut surface. The insert shows a magnification of the curve for $|H_{ext}| \leq 150$ mT.

to prevent any proximity effect. The ferromagnetic crystal [Fig. 1(a)] was grown from a sodium carbonate flux, following a recipe after Ref. 12. When cut along the proper crystallographic axis, single crystals of $BaFe_{12}O_{19}$ exhibit a one-dimensional stripe-type domain structure [Fig. 1(c)] with dominant in-plane magnetization and relatively small out-of-plane component M_z.[13]

To demonstrate that these magnetic domains do not change significantly in perpendicular external magnetic fields $|H_{ext}| \leq 120$ mT, the magnetization M of one slice of the single crystal was measured with a vibrating sample magnetometer as a function of H_{ext} (see Fig. 2). Apparently, the magnetization of the ferromagnet depends almost linearly on the perpendicular applied magnetic field and saturates at $H_{ext} \simeq 1.7$ T. From the slope $dM/dH \sim 3.2 \times 10^5$ Am^{-1} T^{-1}, one can indeed expect only minor changes in the domain structure for $|H_{ext}| \leq 120$ mT, since the corresponding variation in the magnetic moment is less than 7% of the saturated magnetization (5.5×10^5 Am^{-1} T^{-1}). Furthermore, the influence of the external magnetic field on the size and position of the magnetic domains was studied at low temperatures (77 K) with a scanning Hall-Probe microscope.[14] As it is shown in Fig. 3, the width w of the parallel domains increases linearly for $H_{ext} \leq 150$ mT with a rate of approximately 43 nm/mT. In accordance with the very small coercivity of these ferromagnets (see Fig. 2), the observed domain walls returned to their initial positions within the experimental resolution of 1 μm, each time H_{ext} was reduced to zero.

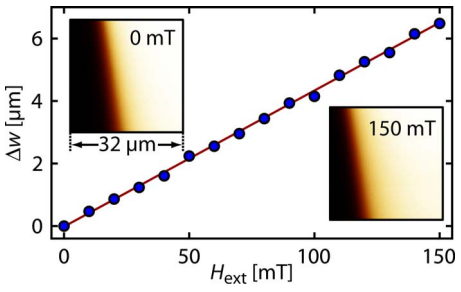

FIG. 3. (Color online) The increase in the width w of a parallel domain (the bright areas in the inserts) in the ferromagnetic substrate as a function of H_{ext}. The shown data is the average of the results obtained for an increasing and a decreasing external magnetic field. The inserts show two examples of the position of the same domain wall at 0 and 150 mT, respectively.

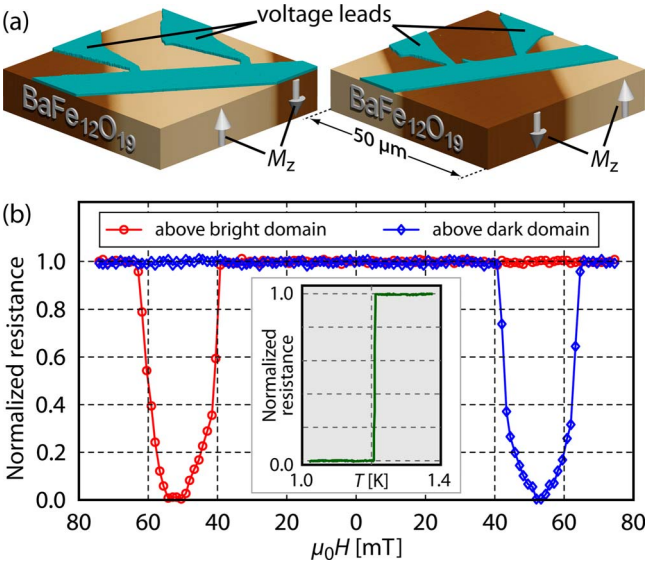

FIG. 4. (Color online) (a) AFM images of two transport bridges with their underlying magnetic domains (MFM images). The MFM images are vertically extended to illustrate the domains. Arrows indicate the z component M_z of the magnetization of the template. (b) The normalized resistance of the two bridges, measured at 340 mK with a bias current of 10 μA as a function of H_{ext}. The insert shows the superconducting transition of a reference Al film on a Si substrate as a function of temperature (critical current density $j_c \sim 1.2 \times 10^8$ A/m^2 at 340 mK).

In order to show that the prepared S/F hybrid systems are suitable for the study of stray field-induced SN interfaces, Fig. 4(b) shows the normalized resistance $R^* := R/R_N$ (R_N being the normal-state resistance) of two transport bridges as a function of H_{ext}. Both curves were measured at 340 mK, i.e., well below the critical temperature $T_c \simeq 1.2$ K of the used aluminum (see the insert of Fig. 4). From the corresponding atomic and magnetic force microscopical images (AFM and MFM, respectively) of Fig. 4(a), it can be seen that the measured parts of the bridges lay entirely above magnetic domains of opposite magnetization. The difference in the MFM signal above the two kinds of domains indicates a nonzero out-of-plane component B^z_{stray} of the stray magnetic field. Note that $B^z_{stray} \neq 0$ above the wide domains results directly from a finite cutting angle φ to the c axis of the crystal. Therefore, by choosing φ, the strength of B^z_{stray} can be adapted to match the critical fields of the superconductor. For the present case, it was found that aluminum as a superconductor and $\varphi = 10°$ are a good match. For the case of the bridge above the bright domain [left panel of Fig. 4(a)], R^* drops to zero around −53 mT (see the red curve with circles). In a symmetric manner, R^* of the bridge above the dark domain shows a similar behavior around +53 mT (see the blue curve with diamonds). These observations prove the possibility to realize the state of RDS by applying compensation fields of $H_{ext} = \pm 53$ mT to the designed $Al/BaFe_{12}O_{19}$ hybrids. Moreover, it becomes clear that in the state of RDS at 340 mK, the superconducting order parameter is completely suppressed above the corresponding parallel domains (i.e., above magnetic domains with magnetization in the same direction as $\vec{H}_{ext}$).

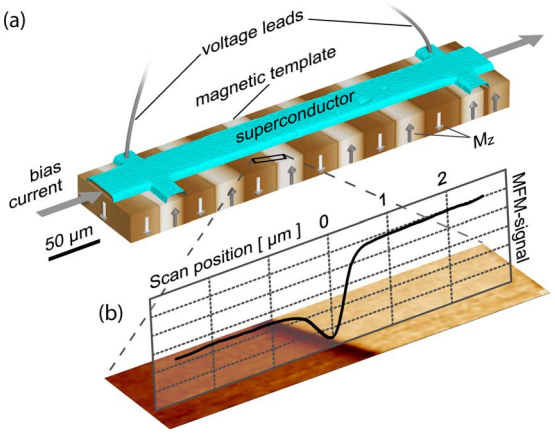

FIG. 5. (Color online) (a) The transport bridge (optical image shown in three dimensions) with its underlying magnetic domains (MFM image). The MFM image is vertically extended to illustrate the domains. Arrows indicate the z component M_z of the magnetization of the template. (b) A detailed MFM image of a typical domain wall in the substrate.

Next, a long transport bridge of 35×250 μm^2 was investigated, which—due to its relatively large size—had to cross several magnetic domain walls of the substrate. Inspection of the sample with a magnetic force microscope revealed indeed nine domain walls underneath the bridge [Fig. 5(a)]. Figure 6 displays the normalized dc resistance of the bridge well below T_c, measured as a function of bias current I and H_{ext}. As can be expected from the above presented results, two pronounced minima in resistivity are seen around ± 53 mT, indicating that stray fields above magnetic domains are compensated by H_{ext}. Application of these compensation fields thus induces the RDS state in the S/F hybrid system. Furthermore, a second key feature can be seen in Fig. 6. While beyond the compensation fields the resistance quickly rises toward its value in the normal state, parts of the

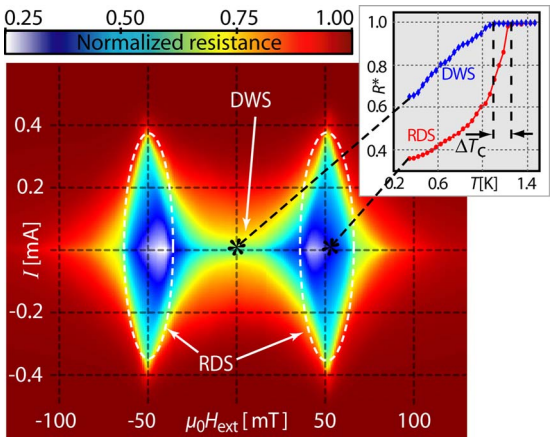

FIG. 6. (Color online) The normalized resistance of the transport bridge of Fig. 5(a) at 340 mK, as a function of bias current I and external field H_{ext} (R_N=3.62 Ω). Regions where RDS and DWS occur are indicated. The insert shows the resistive transitions (I =10 μA) from the normal state to the states of DWS (blue curve with diamonds) and RDS (red curve with circles). The points corresponding to T=340 mK are indicated in the main panel.

bridge remain superconducting when subjected to external fields lower than the compensation fields. Particularly, in the case of zero applied field, when superconductivity is likewise suppressed above domains of opposite magnetization, the reduced resistance is a clear fingerprint of DWS. Moreover, the insert in Fig. 6 shows the transitions of the bridge from the normal state to the states of DWS and RDS (at 0 and 53 mT, respectively) as a function of temperature. The significant difference ΔT_c of the onsets of the transitions reflects the confinement of the superconducting order parameter above wide magnetic domains (RDS) and narrow domain walls (DWS).[15]

Above, the occurrence of the minima in Fig. 6(a) has been discussed, along with the reduction in resistance at zero applied field. However, surprising are the values of the resistance reached at these points: as can be seen from Fig. 5(a), approximately half of the area of the bridge is covered by each kind of domains. Nucleation of superconductivity above one type of domains should thus cause the bridge to loose roughly half of its resistance in the normal state. By contrast, for compensation fields of both polarities, only half of the expected resistance is seen.

A similar observation can be made at H_{ext}=0 when superconductivity survives above domain walls only. In that case, the drop in resistance is, *a priori*, expected to be equal to the ratio between the width of magnetic domains and domain walls. But from detailed MFM studies it becomes clear that all changes in stray fields are confined to approximately 1 μm around domain walls [Fig. 5(b)], whereas the domains are typically 25 μm wide [Fig. 5(a)]. Therefore, in absence of external fields, the observed reduction in resistance by $\sim$45% is surprising.

In order to investigate these remarkable features in more detail, the differential resistance dV/dI of the transport bridge was measured as a function of bias current and temperature in both states, RDS and DWS. Simultaneously, the voltage drop V over the bridge was also detected. Measurements were carried out via standard lock-in techniques at a frequency of 33 Hz and an ac-modulation current of 2 μA. The normalized differential conductance $G_N = \frac{dI}{dV} R_N$ is shown in Fig. 7 as a function of voltage for $H_{ext} = \pm 53$ mT (RDS). In that diagram, results are shown twice for clarity: the left two-dimensional panel displays a few conductance curves that are vertically shifted, whereas all obtained curves are given in a three-dimensional representation at the right. Here, at lowest temperatures, G_N is sharply peaked at zero voltage, declining symmetrically to its minima at $\pm V_1$ before recovering to its normal value at higher voltages. Together with some smaller local minima, these features gradually collapse with increasing temperature.

III. DISCUSSION

In order to interpret the conductance spectra of Fig. 7, several aspects must be taken into account: (i) the whole transport bridge is in the normal state for $|V| > 2$ mV even at the lowest temperature (340 mK). The reason for this is that the critical current density j_c is exceeded due to the low resistance of the bridge. Therefore, in a certain low-voltage

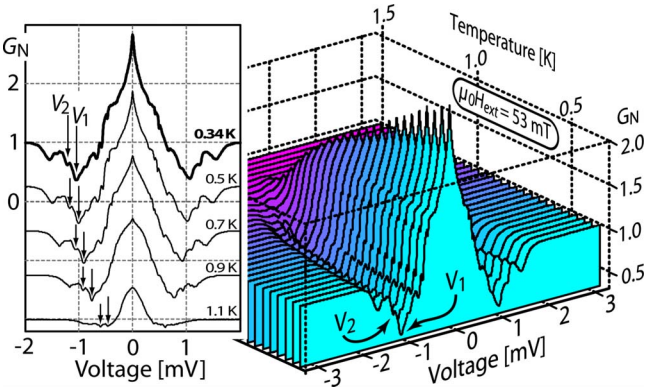

FIG. 7. (Color online) Differential conductance spectra of the transport bridge of Fig. 5(a) at 53 mT in the state of RDS. Arrows mark two minima whose positions can be traced. In the left panel, curves are shifted for clarity and the vertical scale corresponds to the top curve.

region where $j<j_c$, a higher value for G_N is expected since the parts of the bridge above reverse-domains are superconducting. (ii) The normalized differential conductance reaches 2.8 at 340 mK and zero voltage. Assuming that this increase in G_N was solely caused by the N→S transition mentioned under point (i), approximately 64% of the transport bridge had to become superconducting. However, the hybrid system behaves similar for both polarities of H_{ext} (see Fig. 6), meaning that an unequal distribution of parallel and reverse domains cannot be the reason for the high conductances observed at positive *and* negative compensation fields. Moreover, as discussed above, the external field increases the width of the parallel domains by 43 nm/mT (see Fig. 3). Accordingly, at 53 mT, a normalized conductance of only 1.8 instead of 2 should be expected, provided that parallel and reverse domains are equally distributed at $H_{ext}=0$. Finally, the characteristic length $\xi_N=\sqrt{\hbar D/k_B T}$, over which the Cooper pair amplitude decays exponentially with the distance from an SN interface, is in the present case on the order of 400 nm.[16] Due to this proximity effect, the superconducting state extends into the normal regions and vice versa, but the corresponding increase in G_N at $V=0$ is only minor.

Taking account of the above considerations, the observed conductance of 2.8 cannot be explained by a corresponding expansion of the superconducting state along the transport bridge. However, below the superconducting gap Δ (i.e., for $V<\Delta/e$), an excess of the conductance can generally result from Andreev reflection processes at SN interfaces, if the latter are highly transparent for incident electrons. In the present case, normal and superconducting states are created *inside the same material* and, therefore, the presence of highly transparent SN interfaces is reasonable. Accordingly, the observed excess of conductance suggests that the mechanism of charge transfer across the SN interfaces is affected by AR.

The theory of Blonder, Tinkham, and Klapwijk (BTK) (Ref. 17) describes the effects of AR on the conductance of a single SN junction for the particular case of ballistic transport in the normal-state region. From that theory it follows that inside the gap, the conductance can be enhanced up to twice its above-gap value. In the present case, as discussed above, the above-gap conductance in the RDS state at 53 mT can be estimated to be 1.8. Therefore, the observed zero-voltage conductance of 2.8 is smaller than twice the above-gap conductance (2×1.8), meaning that these findings are not in contradiction with the BTK theory.

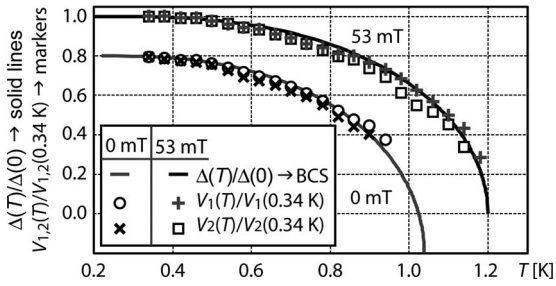

FIG. 8. The positions of characteristic minima in the conductance spectra of Fig. 7 and 9 (markers) are compared with $\Delta(T)$ (solid lines). For clarity, the results obtained at 0 mT are shifted by −0.2.

Moreover, the BTK theory predicts for highly transparent interfaces a flat conductance below the gap, which has been verified experimentally with superconducting point contacts (see, for example, Ref. 18). By contrast, the G_N curves of Fig. 7 are sharply peaked at zero voltage. Such anomalies in the conductance spectra in the form of zero-bias peaks have been reported before in systems that deviate from the model of BTK, such as planar Nb/Au contacts,[19] junctions between superconductors and semiconductors,[20–22] and series of SNS junctions.[23] In the present case, the used sample differs also significantly from the model system of BTK since the bridge crosses nine domain walls [see Fig. 5(a)], each of them inducing one SN interface. Moreover, due to the large size of the domains, the electric transport in the normal-state regions is not ballistic. A theoretical description of such series of diffusive SNS junctions will go beyond the ballistic theories[17,24] and will have to include nonlocal coherent effects in the normal-state regions.[25,26]

(iii) Two of the local minima of the conductance spectra of Fig. 7, marked as V_1 and V_2, can be traced from 340 mK to nearly T_c. Their relative position on the V axis was compared to the superconducting gap function

$$\ln\left(\frac{1.13E_c}{k_B T_c}\right)=\int_0^{E_c}\frac{\tanh(0.5k_B^{-1}T^{-1}\sqrt{\xi^2+\Delta^2})}{\sqrt{\xi^2+\Delta^2}}d\xi$$

of the BCS theory,[27] using a value of 423 K for the ratio between cut-off frequency E_c and Boltzmann constant k_B.[28] A solution $\Delta(T)$ of the above equation can be found by iteration, integrating numerically over energies ξ while treating T_c as a fitting parameter. As illustrated in Fig. 8 (upper curve), $V_{1,2}$ follow strictly the superconducting gap Δ in temperature.

For the ideal case of a single ballistic SNS junction, it is known that multiple Andreev reflection (MAR) leads to minima in the conductance curves at voltages smaller than the gap ($V<\Delta/e$). Their positions follow $\Delta(T)$ in the same way as $V_{1,2}$. However, the present case is quite different in

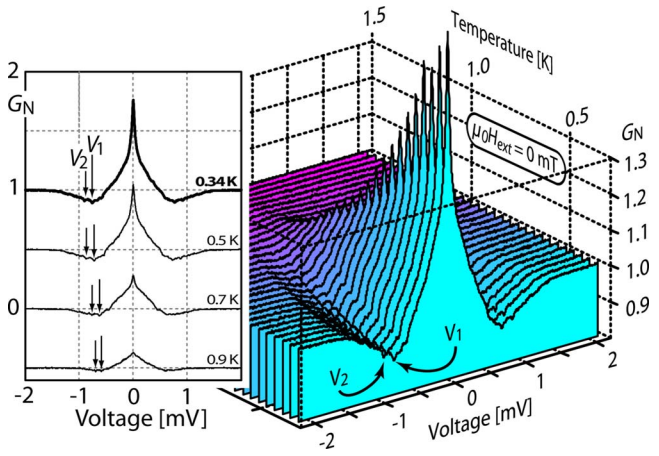

FIG. 9. (Color online) Differential conductance spectra of the transport bridge of Fig. 5(a) at 0 mT (DWS). Arrows mark two minima whose positions can be traced. In the left panel, curves are shifted for clarity and the vertical scale corresponds to the top curve.

that the measured $G(V)$ curves belong to a series of diffusive SNS junctions. When dividing V by the number of SN interfaces[29] and considering that V dropped mainly over the normal-state regions of the bridge, it could be concluded that $V_{1,2}$ lay inside the gap and originate from MAR [typical values for Δ/e are 200 μV for Al (Ref. 30)]. However, it is also possible that series of AR processes lead to multiplication effects and to different effective voltages across subsequent SN interfaces. Therefore, even if caused by the same process, features in $G(V)$ could repeatedly appear at different voltages, and result in the observed set of local minima. Moreover, a multiplication effect in series of junctions might also lead to an increase in the conduction by factors higher than two.[31]

Intriguingly, all observations described above can be made not only in the case of RDS but also in absence of external fields when DWS is realized (Fig. 9). In that case, local minima are less pronounced, but nonetheless, two of them can be traced up to higher temperatures (lower curve in Fig. 8). As before, their positions in the conductance spectra follow the collapse of Δ. It is remarkable that values of T_c obtained by fitting are significantly different in the cases of RDS (1.20 ± 0.02 K) and DWS (1.05 ± 0.03 K). These findings reflect directly that due to quantum size effects, T_c values of superconducting microstructures differ significantly from those of bulk superconductors[32]—an effect that leads to the reduction in T_c when superconductivity is confined above the domain walls of a underlying ferromagnet.[33]

IV. CONCLUSIONS

In conclusion, there are two major findings of this work: on one hand, it has been demonstrated that tunable SN junctions inside superconducting thin films can be created *in a controlled manner* by using magnetic templates. This first conclusion is a direct result from the successful fabrication of a S/F hybrid system, that allows for setting up DWS and RDS in the S-layer, without changing the actual configuration of magnetic domains. On the other hand, the occurrence of Andreev reflection, observed in the conductance of the S layer of the hybrid system, proves the high transparency of SN interfaces induced by magnetic stray fields. This result is based on the innovative approach to create SN junctions *in the same material* via local suppression of superconductivity.

From a technological point of view, generation of SN junctions via ferromagnets is attractive due to both, the natural tunability of magnetic domain structures and the here demonstrated high quality of SN interfaces. Potentially, inclusion of magnetic templates with pure in-plane magnetization will make it possible to invert the scheme of DWS and to *suppress* superconductivity in a very narrow region above domain walls, realizing the domain-wall normal state (DWN). Such configuration may lead to controllable phase-coupling effects between two superconducting reservoirs, separated by a thin DWN region, and pave the way for the development of new types of tunable quantum interference devices.

ACKNOWLEDGMENTS

This work is supported by the Methusalem Funding of the Flemish Government, the FWO, GOA and IAP projects and the ESF-NES Research Networking Programme.

[1] B. D. Josephson, Rev. Mod. Phys. **46**, 251 (1974).
[2] R. Meservey, P. M. Tedrow, and P. Fulde, Phys. Rev. Lett. **25**, 1270 (1970).
[3] A. F. Andreev, Sov. Phys. JETP **19**, 1228 (1964).
[4] In this paper, we use the common term "Andreev reflection," however, it should be noted (Ref. 34) that electron-hole reflection at S/N interfaces was studied independently by de Gennes and Saint-James (Ref. 35) and by Andreev (Ref. 3).
[5] Z. Yang, M. Lange, A. Volodin, R. Szymczak, and V. V. Moshchalkov, Nature Mater. **3**, 793 (2004).
[6] J. Fritzsche, V. V. Moshchalkov, H. Eitel, D. Koelle, R. Kleiner, and R. Szymczak, Phys. Rev. Lett. **96**, 247003 (2006).
[7] A. I. Buzdin, Rev. Mod. Phys. **77**, 935 (2005).
[8] I. F. Lyuksyutov and V. L. Pokrovsky, Adv. Phys. **54**, 67 (2005).
[9] A. Yu. Aladyshkin, A. V. Silhanek, W. Gillijns, and V. V. Moshchalkov, Supercond. Sci. Technol. **22**, 053001 (2009).
[10] A. Belkin, V. Novosad, M. Iavarone, J. Fedor, J. E. Pearson, A. Petrean-Troncalli, and G. Karapetrov, Appl. Phys. Lett. **93**, 072510 (2008).
[11] É. B. Sonin, Pis'ma Zh. Tekh. Fiz. **14**, 1640 (1988).
[12] R. J. Gambino and F. Leonhard, J. Am. Ceram. Soc. **44**, 221 (1961).
[13] A. Hubert and R. Schäfer, *Magnetic Domains* (Springer-Verlag, Berlin, 1998), Chap. 5, p. 403.

[14] S. J. Bending, Adv. Phys. **48**, 449 (1999).
[15] A. Yu. Aladyshkin and V. V. Moshchalkov, Phys. Rev. B **74**, 064503 (2006).
[16] An estimation of the diffusion coefficient is $D=v_F l_p/3 \approx 6.6\cdot 10^{-3}$ m^2/s, with the Fermi velocity $v_F=2.03\times 10^6$ m/s (Ref. 36) and the electron mean-free path $l_p=mv_F/\varrho_i ne^2 \approx 9.8$ nm [m and e are electronic mass and charge, $n=18.1\times 10^{28}$ m^{-3} is the density of conduction electrons (Ref. 36)]. The residual resistance ϱ_i was estimated according to $\varrho_p/\varrho_i+1\approx R(295\ \mathrm{K})/R(1.5\ \mathrm{K})=1.68$, with the resistivity $\varrho_p=2.74\times 10^{-8}$ Ωm of Al at 295 K (Ref. 37).
[17] G. E. Blonder, M. Tinkham, and T. M. Klapwijk, Phys. Rev. B **25**, 4515 (1982).
[18] R. J. Soulen, Jr., J. M. Byers, M. S. Osofsky, B. Nadgorny, T. Ambrose, S. F. Cheng, P. R. Broussard, C. T. Tanaka, J. Nowak, J. S. Moodera, A. Barry, and J. M. D. Coey, Science **282**, 85 (1998).
[19] P. Xiong, G. Xiao, and R. B. Laibowitz, Phys. Rev. Lett. **71**, 1907 (1993).
[20] A. W. Kleinsasser, T. N. Jackson, D. McInturff, F. Rammo, and G. D. Pettit, Appl. Phys. Lett. **57**, 1811 (1990).
[21] C. Nguyen, H. Kroemer, and E. L. Hu, Phys. Rev. Lett. **69**, 2847 (1992).
[22] A. Kastalsky, A. W. Kleinsasser, L. H. Greene, R. Bhat, F. P. Milliken, and J. P. Harbison, Phys. Rev. Lett. **67**, 3026 (1991).
[23] Z. D. Kvon, T. I. Baturina, R. A. Donaton, M. R. Baklanov, K. Maex, E. B. Olshanetsky, A. E. Plotnikov, and J. C. Portal, Phys. Rev. B **61**, 11340 (2000).
[24] M. Octavio, M. Tinkham, G. E. Blonder, and T. M. Klapwijk, Phys. Rev. B **27**, 6739 (1983).
[25] B. J. van Wees, P. de Vries, P. Magnee, and T. M. Klapwijk, Phys. Rev. Lett. **69**, 510 (1992).
[26] Yu. V. Nazarov and T. H. Stoof, Phys. Rev. Lett. **76**, 823 (1996).
[27] T. Tinkham, *Introduction to Superconductivity* (Dover, New York, 1996), Chap. 3, p. 63.
[28] K. A. Gschneidner, Jr., Solid State Phys. **16**, 275 (1964).
[29] T. I. Baturina, D. R. Islamov, and Z. D. Kvon, Sov. Phys. JETP **75**, 326 (2002).
[30] I. Giaever and K. Megerle, Phys. Rev. **122**, 1101 (1961).
[31] L. Shan, H. J. Tao, H. Gao, Z. Z. Li, Z. A. Ren, G. C. Che, and H. H. Wen, Phys. Rev. B **68**, 144510 (2003).
[32] V. V. Moshchalkov, L. Gielen, C. Strunk, R. Jonckheere, X. Qiu, C. Van Haesendonck, and Y. Bruynseraede, Nature (London) **373**, 319 (1995).
[33] W. Gillijns, A. Yu. Aladyshkin, A. V. Silhanek and V. V. Moshchalkov, Phys. Rev. B **76**, 060503(R) (2007).
[34] G. Deutscher, Rev. Mod. Phys. **77**, 109 (2005).
[35] P. de Gennes and D. Saint-James, Phys. Lett. **4**, 151 (1963).
[36] N. W. Ashcroft and N. D. Mermin, *Solid State Physics* (Brooks-Cole, Belmont, 1976), Chap. 2, p. 38.
[37] C. Kittel, *Introduction to Solid State Physics* (John Wiley & Sons, New York, 1976), Chap. 6, p. 171.